

# Reliability-based control optimization for active base isolation systems

J. T. Scruggs<sup>\*,†</sup>, A. A. Taflanidis and J. L. Beck

*Division of Engineering and Applied Science, California Institute of Technology, U.S.A.*

## SUMMARY

A probability-based active control synthesis is proposed for seismic base isolation of a structure that is modeled as a linear dynamical system subjected to uncertain future ground motions that are modeled as a stochastic process. The performance objective is the minimization of the probability of failure, where failure is defined as the first-passage of the system trajectory across a generalized set of hyperplanes in the system response space. Versions of the approach are described for the case with no model uncertainty, as well as for the case with uncertain model parameters with probabilistically distributed values. Numerical issues pertaining to the optimization of the controller are discussed. The method is illustrated in a civil engineering context through application to the eight-storey base isolation benchmark structure model, using an array of ideal active control devices working in tandem with the passive base isolation bearings. Controllers are presented for cases with specified and uncertain earthquake spectral parameters, and for two different actuator configurations. Transient simulations are presented for seven earthquake records, and the performances of the controllers are analyzed under a number of metrics. Comparisons with the performance of a related linear-quadratic controller are presented and discussed, both for stationary as well as transient response. Copyright © 2005 John Wiley & Sons, Ltd.

**KEY WORDS:** structural control; base isolation; first-passage problems; failure minimization; probabilistic uncertainty

## 1. INTRODUCTION

Over the last two decades, there has been a growing interest in the application of active control technologies to civil structures, toward the reduction of seismic risk. The extensive efforts of many researchers have yielded numerous manifestations of this idea, resulting in several distinct actuation strategies and controller designs [1–3]. Of these many approaches, active base isolation systems have emerged as one of the more promising. Because of the growing body of work devoted to these systems, and the inevitable disparity of the various proposed approaches, it is useful to make comparisons on a common example representing a typical application. This has motivated the recent proposal by the ASCE Structural Control Committee of the Base

---

\*Correspondence to: J. T. Scruggs, Division of Engineering and Applied Science, California Institute of Technology, Pasadena, CA 91125, U.S.A.

†E-mail: scruggs@caltech.edu

*Received 17 December 2004*

*Revised 4 April 2005*

*Accepted 28 May 2005*

Isolation Benchmark Control Problem [4], the details of which may also be accessed on the internet at <http://www.ruf.rice.edu/~nagaraja/baseisolationbenchmark.htm>. It consists of an eight-storey irregular structure equipped with passive isolation bearings, which may be fitted with different actuators (both active and semi-active devices may be considered) and controlled through various feedback laws. In addition to a specified structural dynamic model, the problem statement imposes various constraints on the actuators, sensors, and control laws which may be used, and requires that different approaches be compared under a common set of performance measures. As such, a comparison of different base isolation strategies becomes more straightforward.

The motivation for the application of control technology to civil systems, and the metrics by which the quality of such systems are judged, ultimately stems from the concept of system reliability. It stands to reason, then, that the optimal control strategy in such applications should be that which maximizes this reliability. Theoretical reliability-based control methods such as  $H_\infty$  and  $\mu$ -synthesis, and the many offshoots of these, have emerged as the standard tools in the design of feedback controllers which are robust to model uncertainty, where a compact set of possible models for the system is considered. Information implying that some of the possible values of the model parameters are more probable than others is not explicitly treated. However, in most applications, there is considerable engineering knowledge about the relative likelihood of the parameter values. This information can be expressed by specifying probability distributions over the possible values of the parameters. This observation has led to a number of studies involving a probabilistic interpretation of robustness. A sequence of papers by Stengel *et al.* [5–7] addresses the robust stabilization of uncertain systems for which the model uncertainty is characterized through probability density functions on model parameters, and where Monte Carlo simulation was used to converge upon a probabilistic-optimal controller. The idea of probabilistic performance optimization was also investigated by Spencer *et al.* [8], in which FORM/SORM techniques were used to derive an optimal linear controller for a system with probabilistic parameter uncertainty and stochastic excitation.

Another approach [9,10] also deals with a probabilistic treatment of robust stochastic control synthesis. The definition of controller performance used in these studies is motivated by the observation that in civil applications, the ‘failure’ of a control system is related to the probability of first-passage of the system response beyond design thresholds. Such thresholds can be represented as hyperplanes, or ‘failure surfaces’, in the system response space. (Such failure surfaces may be defined to correspond to maximum allowable drifts, accelerations, forces, etc.) In this context, the optimal-reliability controller is the one which minimizes the probability of first-passage across these failure surfaces.

The main contribution of this paper is the application of the above reliability-optimal control design approach to the benchmark base isolation problem. The active control devices used in this study comprise an array of ideal force actuators acting in tandem with the passive isolation bearings. Arrays of both four and eight actuators are considered. The failure criteria consist of thresholds on allowable deformations, accelerations, and forces for the structure–actuator system. For simplicity, four-channel static acceleration feedback is used to give structure to the controller model set over which the optimization is performed. However, in principle, the general procedure considered here can be extended to a much broader class of linear controllers [10].

Section 2 presents an overview of the analytical basis for the approach, the processes involved in designating the failure surfaces, and the numerical issues involved in the convergence to the optimal solution. Section 3 discusses the benchmark base isolation model. Section 4 frames the

proposed probabilistic control optimization in the context of this benchmark model and establishes failure criteria. Section 5 presents simulation results for the benchmark model, and presents some comparisons with performances achieved through linear-quadratic (LQ) optimization methods. Finally, Section 6 draws some conclusions and points toward future work.

## 2. FAILURE SURFACES AND MINIMIZATION OF FAILURE PROBABILITY

### 2.1. Optimal-reliability controllers with known model parameters

Consider a controlled linear system subject to stochastic excitation, i.e.

$$\dot{\mathbf{x}} = \mathbf{A}\mathbf{x} + \mathbf{B}\mathbf{u} + \mathbf{E}\mathbf{a} \quad (1)$$

where  $\mathbf{x} \in \mathfrak{R}^n$  is the state vector,  $\mathbf{u} \in \mathfrak{R}^m$  is the control input, and  $\mathbf{a} \in \mathfrak{R}^p$  is a vector of Gaussian white noise disturbances with spectral intensity  $\Phi_a$ . For a structural model subjected to earthquake excitation, state vector  $\mathbf{x}$  is an augmentation of the structural states, together with states relating to the control law, sensor and actuator dynamics, and the stochastic ground acceleration input model [10]. The dynamics of the sensors and ground acceleration are modeled as linear systems subjected to Gaussian white noise inputs. Thus,  $\mathbf{a}$  is comprised of the noise inputs for both the ground acceleration and the sensor models.

In this paper, we assume a memoryless feedback controller of the form

$$\mathbf{u} = \mathbf{K}\mathbf{C}\mathbf{x} \quad (2)$$

where output feedback matrix  $\mathbf{C} \in \mathfrak{R}^{r \times n}$  selects the observed components of the state, and gain matrix  $\mathbf{K} \in \mathcal{K}$ , where  $\mathcal{K} \subset \mathfrak{R}^{m \times r}$  is the allowed set of controller gain matrices.

First, consider a failure region in the system state space defined by the inequality

$$|y| = |\mathbf{q}^T(\mathbf{K})\mathbf{x}| \geq \beta \quad (3)$$

where the corresponding pair of failure surfaces is the affine subset  $|y| = \beta$  in the state space. Here, it is assumed that the failure surface is linear in  $\mathbf{x}$  and  $\mathbf{u}$ ; i.e.

$$\mathbf{q}(\mathbf{K}) = \mathbf{q}_x + \mathbf{C}^T \mathbf{K}^T \mathbf{q}_u \quad (4)$$

with appropriately-sized vectors  $\mathbf{q}_x$  and  $\mathbf{q}_u$ .

In an interval  $[t, t + dt]$  of infinitesimal width, the probability of ‘out-crossing’ of a system trajectory across the failure surface is given by Rice’s theory [11,12] as  $v_t(\mathbf{K}) dt$ , where  $v_t$  is the out-crossing rate. In stationary response,  $v_t$  is a constant value  $v$ , equal to

$$v(\mathbf{K}) = \frac{\sigma_{\dot{y}}}{\pi\sigma_y} \exp\left[-\frac{1}{2} \frac{\beta^2}{\sigma_y^2}\right] \quad (5)$$

where  $\sigma_y$  and  $\sigma_{\dot{y}}$  are the standard deviations of the Gaussian probability distributions for  $y$  and  $\dot{y}$ . Note that

$$\dot{y} = \mathbf{q}^T(\mathbf{K})[\mathbf{A} + \mathbf{B}\mathbf{K}\mathbf{C}]\mathbf{x} + \mathbf{q}^T(\mathbf{K})\mathbf{E}\mathbf{a} \quad (6)$$

Because  $\mathbf{a}$  is defined as a white noise, and because  $\sigma_{\dot{y}}$  must be finite in order for Equation (5) to be well defined, it is necessary that  $\mathbf{q}(\mathbf{K})$  in Equation (3) be defined such that

$$\mathbf{q}(\mathbf{K}) \perp \mathbf{E} \quad \forall \mathbf{K} \in \mathcal{K} \quad (7)$$

It is then a well-known result of stochastic mechanics that the probability of failure in a finite time interval  $[0, T]$ , under stationary response, can be expressed approximately as

$$\mathcal{P}_{[0, T]}(\mathcal{F} | \mathbf{K}) \cong 1 - \exp[-v(\mathbf{K})T] \quad (8)$$

Here, it has been assumed that  $v \ll 1$ , and  $T$  is much greater than the time constants associated with the closed-loop system. In other words, the approximation is reasonable if failures are unlikely, and if the system response distribution may be assumed to be stationary over most of the interval  $[0, T]$ .

Now consider the case of  $l$  pairs of failure surfaces, each parameterized as in Equation (3) by the set  $\{\mathbf{q}_k(\mathbf{K}), \beta_k\}$  for  $k \in \{1..l\}$ . This is illustrated in Figure 1 for two pairs of surfaces on two states. Thus, we have a vector  $\mathbf{y}$  of performance quantities related to the states and control through

$$\mathbf{y} = \mathbf{C}_y \mathbf{x} + \mathbf{D}_y \mathbf{u} \quad (9)$$

where failure at time  $t$  corresponds to

$$\max_{k \in \{1, \dots, l\}} \{|y_k(t) - \beta_k\} \geq 0 \quad (10)$$

and

$$\mathbf{C}_y = [\mathbf{q}_{x1} \dots \mathbf{q}_{xl}]^T \quad \mathbf{D}_y = [\mathbf{q}_{u1} \dots \mathbf{q}_{ul}]^T \quad (11)$$

Denoting the stationary out-crossing rates for each failure surface  $|y_k(t) - \beta_k$  as  $v_k(\mathbf{K})$ , we have that the total probability of failure in a time window  $[0, T]$  is approximately [13]

$$\mathcal{P}_{[0, T]}(\mathcal{F} | \mathbf{K}) \cong 1 - \exp\left[-\sum_{k=1}^l v_k(\mathbf{K})T\right] = 1 - \exp[-v_{\Sigma}(\mathbf{K})T] \quad (12)$$

where  $v_{\Sigma}(\mathbf{K})$  is the sum of the out-crossing rates for all surfaces. This approximation is justified if the failures are unlikely and not highly correlated. In this context, it follows naturally that an optimal-reliability gain  $\mathbf{K}^*$  will be that gain which minimizes  $\mathcal{P}_{[0, T]}(\mathcal{F} | \mathbf{K})$  over  $\mathbf{K} \in \mathcal{H}$ . For any specified time window, this is equivalent to the minimization of the total out-crossing rate  $v_{\Sigma}(\mathbf{K})$ . Thus, this total out-crossing rate may be viewed as a performance measure to be optimized over

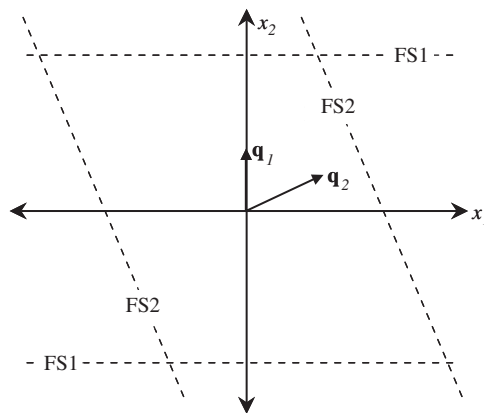


Figure 1. Example of failure surfaces on two states.

the control gain space  $\mathcal{K}$ ; i.e.

$$\mathbf{K}^* = \arg \min_{\mathbf{K} \in \mathcal{K}} \{v_{\Sigma}(\mathbf{K})\} \quad (13)$$

This optimization may be accomplished in a number of ways. The simplest of these involves the incorporation of the gradient  $\partial v_{\Sigma}(\mathbf{K})/\partial \mathbf{K}$  into a first-order ‘steepest-descent’ convergence algorithm. When executed, this approach will converge (very slowly) to a local minimum in  $v_{\Sigma}$ . However, it should be noted that  $v_{\Sigma}(\mathbf{K})$  is in general nonconvex, and hence may have many local minima in  $\mathcal{K}$ . The development of efficient global optimization methods for this problem is still under investigation.

Some care must be taken in the designation of failure surfaces, and the above discussion does not address all the aspects of this process. For instance, the optimizing  $\mathbf{K}^*$  should imply stability for the entire state space. This condition is not implied by the above discussion, but can be ensured by placing certain detectability constraints on  $\mathbf{C}_y$  and  $\mathbf{D}_y$ . Additionally, in order for approximation (12) to hold, the failure surfaces should be chosen such that there is a low correlation between any two failures, which again places constraints on the  $\mathbf{C}_y$  and  $\mathbf{D}_y$ , as well as  $\beta$ . While important, these issues are beyond the scope of this paper, the purpose of which is primarily demonstrative. They will be addressed in a separate forthcoming paper.

## 2.2. Probabilistic model uncertainty

Realistically, any model used for the development of a structural controller will have some parametric uncertainty, which may stem from multiple sources. Clearly, there will be some uncertainty associated with the structural model. However, it is arguable that the uncertainty in the stochastic ground acceleration model is the more dominant source. In this study, the earthquake acceleration is incorporated into Equation (1) as a filter that shapes white noise. There exists a great degree of uncertainty as to the appropriate spectral characteristics of this filter to represent possible ground motions at the structural site. This may be incorporated into Equation (8) as a probabilistic uncertainty on the filter parameters associated with the earthquake ground motion model.

Let the vector of these uncertain model parameters be denoted  $\theta \in \Theta$ , where  $\Theta \subset \mathfrak{R}^h$  denotes the model class chosen for the problem, and may in general be a non-compact set. The uncertainty in  $\theta$  is modeled by the PDF  $p(\theta | \Theta)$ . Thus, the total probability of failure for a given controller  $\mathbf{K}$  is denoted

$$\begin{aligned} \mathcal{P}_{[0,T]}(\mathcal{F} | \mathbf{K}, \Theta) &= \int_{\Theta} \mathcal{P}_{[0,T]}(\mathcal{F} | \mathbf{K}, \theta) p(\theta | \Theta) d\theta \\ &= 1 - \int_{\Theta} \exp(-v_{\Sigma}(\mathbf{K}, \theta)T) p(\theta | \Theta) d\theta \end{aligned} \quad (14)$$

and thus the probabilistic failure-optimal controller may be found as

$$\mathbf{K}^* = \arg \max_{\mathbf{K} \in \mathcal{K}} \left\{ \int_{\Theta} \exp(-v_{\Sigma}(\mathbf{K}, \theta)T) p(\theta | \Theta) d\theta \right\} \quad (15)$$

Note that Equation (15) is *not* equivalent to a minimization of the mean of  $v_{\Sigma}$  over  $\Theta$ .

The evaluation of the integral in Equation (15) must in general be performed numerically, and this is nontrivial because its dimension grows with the number of uncertain parameters, and because the typical failure rates considered in this analysis are very low. To approximate the

integral, we here follow the methods in [9,10], which entails fitting a Gaussian distribution to the integrand about a maximal design point. Specifically, define

$$s(\mathbf{K}, \boldsymbol{\theta}) = -v_{\Sigma}(\mathbf{K}, \boldsymbol{\theta})T + \log p(\boldsymbol{\theta}|\Theta) \quad (16)$$

Then it follows that the parameter  $\boldsymbol{\theta}^* \in \Theta$  which maximizes Equation (16) also maximizes the integrand of Equation (15). Using a second-order Taylor series expansion of Equation (16) about  $\boldsymbol{\theta}^*$ , the integrand of Equation (15) is approximately a Gaussian distribution with mean  $\boldsymbol{\theta}^*$ , so the integral is approximately

$$\int_{\Theta} \exp(-v_{\Sigma}(\mathbf{K}, \boldsymbol{\theta})T) p(\boldsymbol{\theta} | \Theta) d\boldsymbol{\theta} \cong (2\pi)^{h/2} \frac{\exp[-v_{\Sigma}(\mathbf{K}, \boldsymbol{\theta}^*)T] p(\boldsymbol{\theta}^* | \Theta)}{\sqrt{\det\{\mathbf{H}(\mathbf{K}, \boldsymbol{\theta}^*)\}}} \quad (17)$$

where  $\mathbf{H}(\mathbf{K}, \boldsymbol{\theta}) = -\nabla_{\boldsymbol{\theta}} \nabla_{\boldsymbol{\theta}} s$  is the negative of the negative-definite Hessian matrix with respect to  $\boldsymbol{\theta}$ . Details concerning the derivation of this result can be found in the literature [14].

Thus, the probabilistic optimal-reliability controller can be approximately found through two simultaneous optimizations:

$$\begin{aligned} \mathbf{K}^* &= \arg \max_{\mathbf{K} \in \mathcal{K}} \left\{ \frac{\exp[-v_{\Sigma}(\mathbf{K}, \boldsymbol{\theta}^*)T] p(\boldsymbol{\theta}^* | \Theta)}{\sqrt{\det(\mathbf{H}(\mathbf{K}, \boldsymbol{\theta}^*))}} \right\} \\ \boldsymbol{\theta}^* &= \arg \max_{\boldsymbol{\theta} \in \Theta} \{-v_{\Sigma}(\mathbf{K}^*, \boldsymbol{\theta})T + \log p(\boldsymbol{\theta} | \Theta)\} \end{aligned} \quad (18)$$

Efficient optimization routines for this problem remain an item of ongoing research. In this paper, the optimization is carried out using MATLAB [15] optimization functions `fmins()`, which employs a Nelder–Mead nonlinear simplex algorithm, and `fmincon()`, which uses a more elaborate convergence method. It is acknowledged that there is no guarantee that the global maximum of the two optimization problems is attained; in practice, the optimization algorithm will converge to a local maximum near the starting value.

### 3. THE BASE ISOLATION BENCHMARK CONTROL PROBLEM

The benchmark structural model represents a base-isolated structure with  $n_f = 8$  floors, with the horizontal  $x$  and  $y$  coordinates for the  $i$ th floor denoted as  $x_{is}^i$  and  $y_{is}^i$ , respectively. There are  $n_b = 92$  bearings and  $n_c$  actuators between the base and the ground, with  $x$  and  $y$  coordinates for the  $i$ th actuator denoted  $x_c^i$  and  $y_c^i$ , respectively. The superstructure is a linear elastic system. The base and floor slabs are assumed to be infinitely rigid in plane and are modeled by three master degrees of freedom (two horizontal and one rotational about the vertical axis) located at the centers of mass of each floor.

#### 3.1. Design model description

The structural model has mass, damping and stiffness matrices  $\mathbf{M}_p$ ,  $\mathbf{C}_p$ , and  $\mathbf{K}_p$ . The differential equation for the coordinate vector  $\mathbf{p}$  (consisting of the lateral and rotational displacements for each floor as well as the base) can be expressed as

$$\mathbf{M}_p \ddot{\mathbf{p}} + \mathbf{C}_p \dot{\mathbf{p}} + \mathbf{K}_p \mathbf{p} = \begin{bmatrix} \mathbf{0}_{3n_f \times 3} \\ \mathbf{I} \end{bmatrix} \mathbf{u}_f + \begin{bmatrix} \mathbf{M}_s \mathbf{R} \\ \mathbf{R}^T \mathbf{M}_s \mathbf{R} + \mathbf{M}_b \end{bmatrix} \begin{bmatrix} \ddot{\mathbf{x}}_g \\ 0 \end{bmatrix} \quad (19)$$

where  $\ddot{\mathbf{x}}_g \in \mathfrak{R}^2$  is the acceleration of the ground in the  $x$  and  $y$  directions. Vector  $\mathbf{u}_f \in \mathfrak{R}^3$  contains the total control forces on the base in the  $x$  and  $y$  directions and the total control torque about the base center of mass. Matrix  $\mathbf{R} = [\mathbf{r}^{n_t} \dots \mathbf{r}^1]^T$  is the  $3n_t \times 3$  matrix of earthquake influence coefficients, where matrices  $\mathbf{r}^i$  are defined as

$$\mathbf{r}^i = \begin{bmatrix} 1 & 0 & y_r^i \\ 0 & 1 & -x_r^i \\ 0 & 0 & 1 \end{bmatrix} \tag{20}$$

where  $\{x_r^i, y_r^i\}$  is the position of the center of mass of the  $i$ th floor with respect to the center of mass of the base.

Acceleration  $\ddot{\mathbf{x}}_g$  is modeled by a zero-mean stationary Gaussian process, represented as

$$\dot{\mathbf{w}} = \mathbf{A}_g \mathbf{w} + \mathbf{B}_g \mathbf{a}_g, \quad \ddot{\mathbf{x}}_g = \mathbf{C}_g \mathbf{w} \tag{21}$$

where  $\mathbf{a}_g$  is a Gaussian white noise excitation vector in the  $x$  and  $y$  directions, with diagonal spectral density  $\Phi_g$ . The filtered noise is assumed to have a Kanai–Tajimi-like spectrum, parameterized by  $\zeta_g$  and  $\omega_g$  as

$$\mathbf{A}_g = \begin{bmatrix} \mathbf{0}_{2 \times 2} & \mathbf{I}_2 \\ -\omega_g^2 \mathbf{I}_2 & -2\omega_g \zeta_g \mathbf{I}_2 \end{bmatrix}, \quad \mathbf{B}_g = \begin{bmatrix} \mathbf{0}_{2 \times 2} \\ \mathbf{I}_2 \end{bmatrix}, \quad \mathbf{C}_g = [\mathbf{0}_{2 \times 2} \quad 4\zeta_g \omega_g \mathbf{I}_2] \tag{22}$$

and with equal noise intensity in both directions; i.e.  $\Phi_g = \phi_g \mathbf{I}_2$ .

### 3.2. Filtered accelerations for failure criteria

Recall that for the computation of the failure probabilities, Equation (7) must hold. However, if some of the failure surfaces correspond to the absolute accelerations of various degrees of freedom, this equation will be violated. This problem can be circumvented by using low-pass-filtered estimates of these accelerations in the failure criteria [9], through the differential equation

$$\begin{aligned} \dot{\mathbf{x}}_a &= \mathbf{A}_a \mathbf{x}_a + \mathbf{B}_a \mathbf{z}_a \\ \tilde{\mathbf{z}}_a &= \mathbf{C}_a \mathbf{x}_a \end{aligned} \tag{23}$$

where vector  $\mathbf{z}_a \in \mathfrak{R}^l$  contains acceleration quantities for each failure surface  $k \in \{1..l\}$  (some may be zero), and  $\tilde{\mathbf{z}}_a$  contains the filtered values. Matrices  $\mathbf{A}_a$ ,  $\mathbf{B}_a$ , and  $\mathbf{C}_a$  correspond to a low-pass filter with bandwidth 30 Hz and damping ratio 0.707.

### 3.3. Acceleration feedback

The controllers considered in this study employ filtered acceleration feedback. For  $r$  acceleration feedback measurements, define  $\mathbf{z}_c \in \mathfrak{R}^r$  to be the vector of the actual accelerations at the accelerometer locations, and  $\tilde{\mathbf{z}}_c$  as the corresponding filtered values used in the controller. Then the control force vector  $\mathbf{u}_f$  is related to  $\tilde{\mathbf{z}}_c$  through control gain  $\mathbf{K}_f$  as

$$\mathbf{u}_f = \mathbf{K}_f \tilde{\mathbf{z}}_c \tag{24}$$

In this example, accelerometers are located at the base and the eighth floor, in both  $x$  and  $y$  directions (i.e.  $r = 4$ ). Thus,  $\mathbf{K}_f$  is a  $3 \times 4$  matrix.

The acceleration filter can be viewed as the consequence of the mechanical dynamics of the accelerometers and the chosen dynamics in the control law. Each filter is modeled as second-order low-pass filter with bandwidth  $\omega_c$  and damping  $\zeta_c$ . It is assumed that all filters have the same filter parameters. The bandwidth  $\omega_c$  is treated as a design parameter in the controller (i.e. it is included in the  $\mathbf{K}$  matrix), while  $\zeta_c$  is designated as 0.707. To formalize these ideas, the acceleration feedback dynamics in the controller can be expressed as

$$\begin{aligned}\dot{\mathbf{x}}_c &= \mathbf{A}_c \mathbf{x}_c + \mathbf{B}_c (\mathbf{K}_c \mathbf{x}_c + \mathbf{z}_c + \mathbf{a}_c) \\ \tilde{\mathbf{z}}_c &= \omega_c^2 \mathbf{C}_c \mathbf{x}_c\end{aligned}\quad (25)$$

where  $\mathbf{x}_c$  is the internal state of the controller,  $\mathbf{a}_c$  represents sensor noise modeled as white noise with spectral density  $\Phi_c$ , and where

$$\mathbf{A}_c = \begin{bmatrix} \mathbf{0}_{r \times r} & \mathbf{I}_r \\ \mathbf{0}_{r \times r} & \mathbf{0}_{r \times r} \end{bmatrix} \quad \mathbf{B}_c = \begin{bmatrix} \mathbf{0}_{r \times r} \\ \mathbf{I}_r \end{bmatrix} \quad \mathbf{C}_c = [\mathbf{I}_r \quad \mathbf{0}_{r \times r}] \quad \mathbf{K}_c = [-\omega_c^2 \mathbf{I} \quad -2\zeta_c \omega_c \mathbf{I}]$$

Formulated as such,  $\mathbf{K}_c$  is treated as a feedback control gain, which can be varied to reflect different values of  $\omega_c$ .

The total control input vector  $\mathbf{u}$  is comprised of the structural forces  $\mathbf{u}_f$ , and the ‘control inputs’  $\mathbf{K}_c \mathbf{x}_c$  to the acceleration filters. It follows that the total feedback control gain  $\mathbf{K}$  relates  $\mathbf{x}_c$  to  $\mathbf{u}$  as

$$\mathbf{u} = \begin{bmatrix} \mathbf{K}_f \tilde{\mathbf{z}}_c \\ \mathbf{K}_c \mathbf{x}_c \end{bmatrix} = \mathbf{K} \mathbf{x}_c \quad (26)$$

where  $\mathbf{K}$  has the structure

$$\mathbf{K} = \begin{bmatrix} \omega_c^2 \mathbf{K}_f & \mathbf{0} \\ -\omega_c^2 \mathbf{I} & -2\zeta_c \omega_c \mathbf{I} \end{bmatrix} \quad (27)$$

### 3.4. The augmented system

The entire  $n$ -state system can be placed in the form of Equations (1) and (2) through the augmentation of Equations (21), (23), and (25), with the entire state vector represented as

$$\mathbf{x} = [\mathbf{p}^T \quad \dot{\mathbf{p}}^T \quad \mathbf{w}^T \quad \mathbf{x}_a^T \quad \mathbf{x}_c^T]^T \quad (28)$$

and with appropriate definitions for  $\mathbf{A}$ ,  $\mathbf{B}$ , and  $\mathbf{E}$ . For the purpose of control system design, this linear model was used. However, for simulations to evaluate controller performance, some nonlinearities were imposed. As shown in Figure 2, the model incorporates actuator and sensor

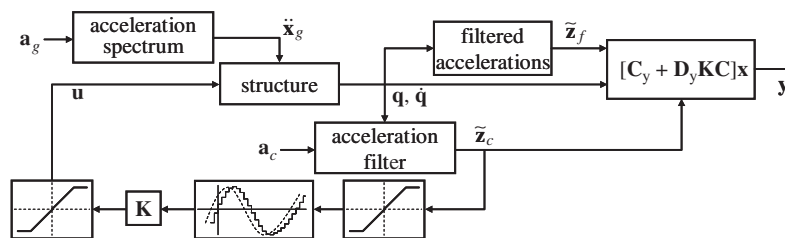


Figure 2. Block diagram of simulated system.

saturation, time delays and discretization errors. Additionally, the acceleration filter in Equation (25) is mapped to an equivalent discrete-time representation, assuming zero-order-hold A/D input conversion and a sampling interval of 5 ms. The values adopted for all these parameters are the ones suggested in the problem definition [4]. The entire system is simulated in SIMULINK [16] with a numerical time step of 5 ms.

### 3.5. Model uncertainty

Uncertainty is considered only in the model parameters for the spectrum of the ground acceleration; i.e.  $\omega_g$ ,  $\zeta_g$  and  $\phi_g$ . The probability density functions chosen to model the uncertain input parameters are

- $\omega_g$  is log-normally distributed with mean  $2\pi$  rad/s and  $\sigma_{\log\omega} = 0.5$
- $\zeta_g$  is log-normally distributed with mean 0.3 and  $\sigma_{\log\zeta} = 0.2$
- $\phi_g$  is log-normally distributed with mean 1 and  $\sigma_{\log\phi} = 0.3$

The choice of the particular PDFs to model the uncertainty in the ground motion model is somewhat arbitrary. However, the total failure probability does not depend strongly on the form of the probability models, provided different choices for these models have similar most probable values and similarly small curvatures for their distributions at that point, because the value of the integral in Equation (14) is largely determined by the behavior of the integrand near its peak.

For the parameters of the PDFs, effort was made such that the distribution for the earthquake spectrum roughly matches that of the set of the earthquake ground motions considered, and the mean values for the parameters are equal to the ones adopted in the benchmark problem statement [4].

### 3.6. Evaluation criteria

The benchmark problem statement defines nine evaluation criteria which represent measures of different RMS and maximum responses of the buildings for seven different earthquakes. Evaluation criteria  $J_1$  and  $J_2$  represent the peak base shear at isolation level and the structure shear at the first story level.  $J_3$  is the peak base displacement,  $J_4$  is the peak inter-storey drift, and  $J_5$  is the peak absolute floor acceleration.  $J_7$  and  $J_8$  are the RMS values of base displacement and interstorey drift. In all the above cases, the performance measures are normalized by the corresponding quantities in the uncontrolled structure. Finally,  $J_6$  represents the force generated by all control devices normalized by the peak base shear in the controlled structure, and  $J_9$  is the total energy absorbed by all control devices normalized by the energy input in the controlled structure.

In addition to these nine criteria, a tenth criterion  $J_{10}$  is included in the results for this study. This additional criterion is equal to the maximum *corner* drift for the controlled structure, normalized by the maximum for the uncontrolled case. Comparisons with  $J_4$  give an indication of the total reduction in the twisting of the building.

## 4. CONTROLLER DESIGN

In this paper, two actuator configurations are considered; one with 4 actuators in each direction (i.e.  $n_c = 8$ ) at corners 3, 13, 19 and 31, and the other with 8 actuators in each direction

(i.e.  $n_c = 16$ ) at positions 3, 8, 13, 19, 24, 26, 31 and 45. (See [4] for these locations.) In both cases, the maximum capacity of each actuator is 2200 kN.

Four different controllers are designed for the benchmark problem. The first two correspond to the four-actuator case. The first one is designed to minimize the failure probability for a particular excitation model. Mean values are adopted for the excitation filter parameters and this case is called the ‘four-actuator nominal-model controller’ or 4NC. The second controller is designed to minimize the total failure probability. This controller, called the ‘four-actuator probabilistic model controller’ or 4PC, incorporates the probability models for the uncertainty of the excitation model parameters. The third and fourth cases correspond to analogous optimizations with the eight-actuator configuration, and will thus be referred to as the 8NC and 8PC cases.

#### 4.1. Determination of actuator forces

As mentioned, the control input  $\mathbf{u}_f \in \mathfrak{R}^3$  corresponds to the *total* forces in  $x$ - and  $y$ -directions, and the *total* moment about the center of mass of the base due to all actuators. Let  $\mathbf{f}_c$  be the vector of forces produced by each individual device. Then  $\mathbf{f}_c$  and  $\mathbf{u}_f$  are related by

$$\mathbf{u}_f = \mathbf{R}_c \mathbf{f}_c \quad (29)$$

where

$$\mathbf{R}_c = [\mathbf{r}_c^1 \ \dots \ \mathbf{r}_c^{n_c}] \quad \text{where } \mathbf{r}_c^i = \begin{cases} [1 \ 0 \ -y_c^i]^T & \text{(actuator in the } x\text{-direction)} \\ [0 \ 1 \ x_c^i]^T & \text{(actuator in the } y\text{-direction)} \end{cases} \quad (30)$$

Assuming at least three actuators simultaneously do not align with each other or with the center of mass,  $\mathbf{R}_c$  has rank 3. If more than three actuators are used,  $\mathbf{R}_c$  has a nontrivial null space, and thus Equation (29) has infinite solutions for  $\mathbf{f}_c$ , given  $\mathbf{u}_f$ . An optimum force distribution may be derived by using the right generalized inverse of  $\mathbf{R}_c$ . Defining this generalized inverse as  $\mathbf{T}$ , it is equal to

$$\mathbf{T} = \mathbf{R}_c^T (\mathbf{R}_c \mathbf{R}_c^T)^{-1} \quad (31)$$

Thus, for  $\mathbf{u}_f$  as in Equation (2), one solution for  $\mathbf{f}_c$  can be related to the states as

$$\mathbf{f}_c = \mathbf{T} \mathbf{K}_f \mathbf{C}_f \mathbf{x} \quad (32)$$

for  $\mathbf{C}_f$  appropriately defined. This produces the minimum-Euclidean-norm  $\mathbf{f}_c$  for a given control gain  $\mathbf{K}_f$ .

#### 4.2. Designation of failure surfaces

The vector  $\mathbf{y}$  of performance quantities is expressed as in Equation (9) with appropriate definitions for  $\mathbf{C}_y$  and  $\mathbf{D}_y$ . In this example, these matrices are such that  $\mathbf{y}$  consists of:

1. The drifts for the base and all stories, measured at the outermost corners
2. The absolute accelerations of the eighth floor and the base in  $x$  and  $y$  directions
3. Three failure quantities related to the actuator forces

The first two items above can be related to the state vector  $\mathbf{x}$  as described in the previous section. For the structural drifts, the failure thresholds are chosen to be 1% of the storey height. For the accelerations, the failure threshold is chosen as 0.6 g. For the base displacement, the

threshold is 0.6 m. These chosen values may be somewhat larger than typical ones which might be used in structural design, but if smaller failure thresholds are chosen, closed-loop failures may occur so frequently (for all controllers) that the approximations leading to Equation (12) are unreasonable.

To explain the specification of force failure thresholds requires a more in-depth discussion. If an actuator is commanded to realize a force beyond its maximum force rating  $f_{\max}$  (equal to 2200 kN in this example), a command limiter imposes a saturation on the actual force realized by the device. Thus, the imposition of actuator failure surfaces on the control optimization should be viewed as a means of discriminating against  $\mathbf{K}_f$  values which have a high probability of saturation.

Ideally, ‘actuator failure’ could be defined by  $n_c$  force failure regions (i.e. one corresponding to the  $x$ - and  $y$ -direction of each actuator) of the form

$$|f_{ci}| \geq \gamma f_{\max} \quad i \in \{1, \dots, n_c\} \quad (33)$$

Quantity  $\gamma > 1$  is a design parameter, that reflects the empirical observation that a small degree of force saturation does not significantly affect the performance of the controller and that  $\gamma = 1$  consequently yields controllers which are overly conservative.

However, it turns out that the above approach does not adhere to necessary conditions for the approximation in Equation (12) to be justified. This is because all  $n_c$  forces in  $\mathbf{f}_c$  are related to only three control inputs  $\mathbf{u}_f \in \mathfrak{R}^3$ , and thus are composed of only three independent random variables. Consequently, there will be a significant correlation between the failures of the various surfaces described above, even if these failures are highly unlikely.

One way to address this problem is through the use of singular values. Let  $\mathbf{V} \in \mathfrak{R}^{3 \times 3}$  be the right-hand unitary transformation matrix corresponding to the singular value decomposition of  $\mathbf{T}$ , and let  $\mathbf{\Sigma} \in \mathfrak{R}^{3 \times 3}$  be the diagonal matrix of nonzero singular values. Then the isometry  $\|\mathbf{\Sigma V}^T \mathbf{u}_f\|_2 = \|\mathbf{f}_c\|_2$  holds, as well as the inequalities

$$\begin{aligned} \|\mathbf{f}_c\|_\infty &\leq \|\mathbf{f}_c\|_2 \leq \sqrt{n_c} \|\mathbf{f}_c\|_\infty \\ \|\mathbf{\Sigma V}^T \mathbf{u}_f\|_\infty &\leq \|\mathbf{\Sigma V}^T \mathbf{u}_f\|_2 \leq \sqrt{3} \|\mathbf{\Sigma V}^T \mathbf{u}_f\|_\infty \end{aligned} \quad (34)$$

which imply

$$\begin{aligned} |\Sigma_i \mathbf{v}_i^T \mathbf{u}_f| &\leq \frac{1}{\sqrt{3}} \gamma f_{\max} \quad \forall i \in \{1, 2, 3\} \Rightarrow \|\mathbf{f}_c\|_\infty \leq \gamma f_{\max} \\ |\Sigma_i \mathbf{v}_i^T \mathbf{u}_f| &\geq \sqrt{n_c} \gamma f_{\max} \quad \text{any } i \in \{1, 2, 3\} \Rightarrow \|\mathbf{f}_c\|_\infty \geq \gamma f_{\max} \end{aligned} \quad (35)$$

where  $\mathbf{v}_i$  is the  $i$ th column of  $\mathbf{V}$ , and  $\Sigma_i$  the corresponding singular value. Thus, the first line in Equation (35) corresponds to a conservative failure criterion, while the second corresponds to a liberal criterion. The design approach adopted here was therefore to prescribe three failure surfaces that lie in between these two constraints; i.e.

$$|\Sigma_i \mathbf{v}_i^T \mathbf{u}_f| \leq \alpha \gamma f_{\max} \quad \alpha \in \left[ \frac{1}{\sqrt{3}}, \sqrt{n_c} \right] \quad (36)$$

where  $\alpha$  is a design parameter. After some trial and error, the values of  $\alpha$  and  $\gamma$  for this example were chosen to be 2.3 and 1.4 for all design cases.

### 4.3. Optimization procedure

The design of the controller in each case consists of the optimization of the 13 independent parameters in Equation (27) for  $\mathbf{K}$  (i.e. the  $3 \times 4$  matrix  $\mathbf{K}_f$ , and parameter  $\omega_c$ ). This optimization is implemented using the optimization toolbox of MATLAB. For better accuracy, the optimization is performed over four successive steps, including more parameters at each step and using the optimal results of the previous step as initial values.

For probabilistic control designs 4PC and 8PC, a final time  $T$  must be specified for the optimization in Equation (18). A choice of  $T$  which is too large or small will result in a dramatic reduction in the sensitivity of  $\mathcal{P}(\mathcal{F} | \mathbf{K}, \Theta)$  to  $\mathbf{K}$  because the failure probabilities for all stabilizing controllers congregate near one (for  $T$  large) or zero (for  $T$  small). This can create numerical problems in the optimization and consequently, a reasonable choice for  $T$  must be found through some trial-and-error. For this example,  $T$  was chosen to be 30 s.

### 4.4. Equivalent LQ controllers

When analyzing the efficacy of the controllers designed in this study, it is instructive to compare their performance to an equivalent linear-quadratic optimal controller, designed under the nominal model parameters. Such a controller can be found through the optimization of  $\mathbf{K}$  over the same controller space  $\mathcal{K}$ , but in reference to a quadratic performance functional on  $\mathbf{y}$ , rather than a failure-based performance measure. To make a fair comparison, these functionals should be somehow 'equivalent'. Here, this is done by assuming the quadratic functional to be a summation of the variances of the components of  $\mathbf{y}$ , normalized by their failure thresholds  $\boldsymbol{\beta}$ ; i.e.

$$\mathbf{K}_{\text{LQ}}^* = \arg \min_{\mathbf{K} \in \mathcal{K}} \left\{ \sum_{i=1}^l \left( \frac{\sigma_{y_i}}{\beta_i} \right)^2 \right\} \quad (37)$$

In control theory, such an optimization is often called 'fixed-structure' in reference to the fact that the optimization is restricted to a fixed controller model structure. Procedures for such optimizations are well known in the literature [17] and, in the interest of brevity, will not be repeated here.

## 5. RESULTS

### 5.1. Failure statistics

For the 4NC, 4PC, 8NC, and 8PC controller designs, as well as the equivalent LQ controllers (here denoted 4LQ and 8LQ), Table I shows selected performance data for the closed-loop stationary response. It turns out that for all cases, the only failure rates which are non-negligible are those of the base drifts and those of force failure surfaces 1 and 2 (i.e. the  $\mathbf{u}$  failure surfaces corresponding to the two highest singular values of  $\mathbf{T}$ ). All others are at least an order of magnitude smaller and are not included in the table.

Consider first the four-actuator case. As expected, the 4NC case yields a lower failure rate than the 4LQ case, with a margin of improvement of about 8%. This illustrates an underlying observation of this study, which is that *linear-quadratic controllers are not necessarily the best controllers for failure reduction*. Note that this observation is buttressed by the eight-actuator case, where the improvement in failure rate between the 8LQ and 8NC cases is around 19%.

Now, consider the last column in the table, labeled ‘failure probability’. These probabilities correspond to the evaluation of Equation (14) for each controller. Note that although the NC case improves significantly upon the LQ case for the nominal model for both four and eight actuators, as measured by the improvement in the total failure rate, the total failure probabilities

Table I. Failure statistics for various controller designs.

Controller	Failure rates					Failure probability $\mathcal{P}_{[0,T]}(\mathcal{F})$
	Base displacement		u-space surfaces			
	$v_x$	$v_y$	$v_1$	$v_2$	$v_\Sigma$	
8LQ	0.0093	0.0038	0.0001	0.0016	0.0148	0.657
8NC	0.0061	0.0032	0.0010	0.0016	0.0118	0.652
8PC	0.0046	0.0021	0.0074	0.0080	0.0226	0.615
4LQ	0.0195	0.0085	0.0022	0.0008	0.0310	0.695
4NC	0.0145	0.0073	0.0042	0.0026	0.0286	0.681
4PC	0.0102	0.0059	0.0101	0.0064	0.0327	0.657

Table II. Performance data for FP-x case (four actuators).

Simulation case		$J_1$	$J_2$	$J_3$	$J_4$	$J_5$	$J_6$	$J_7$	$J_8$	$J_9$	$J_{10}$
Newhall	LQ	0.791	0.805	0.775	0.766	0.749	0.306	0.465	0.600	0.692	0.771
	NC	0.787	0.800	0.722	0.761	0.744	0.308	0.424	0.568	0.710	0.768
	PC	0.778	0.791	0.657	0.751	0.733	0.312	0.384	0.533	0.723	0.758
Slymar	LQ	0.731	0.744	0.684	0.711	0.816	0.219	0.429	0.534	0.718	0.722
	NC	0.742	0.756	0.654	0.690	0.820	0.216	0.428	0.540	0.732	0.698
	PC	0.756	0.772	0.621	0.716	0.870	0.212	0.428	0.549	0.745	0.713
El Centro	LQ	0.815	0.797	0.503	0.707	0.729	0.263	0.458	0.424	0.611	0.522
	NC	0.797	0.777	0.484	0.685	0.708	0.304	0.435	0.407	0.643	0.510
	PC	0.778	0.757	0.473	0.667	0.690	0.348	0.419	0.396	0.671	0.493
Rinaldi	LQ	0.902	0.904	0.636	0.897	0.921	0.203	0.404	0.463	0.695	0.813
	NC	0.899	0.901	0.631	0.894	0.918	0.204	0.392	0.455	0.713	0.812
	PC	0.891	0.893	0.617	0.887	0.911	0.205	0.376	0.447	0.730	0.806
Kobe	LQ	0.673	0.668	0.539	0.647	0.902	0.222	0.491	0.449	0.598	0.665
	NC	0.677	0.672	0.497	0.639	0.895	0.245	0.452	0.419	0.612	0.661
	PC	0.673	0.668	0.442	0.631	0.886	0.271	0.423	0.400	0.623	0.650
Jiji	LQ	0.881	0.875	0.873	0.866	0.893	0.101	0.627	0.740	0.505	0.720
	NC	0.877	0.863	0.867	0.883	0.925	0.102	0.623	0.753	0.509	0.770
	PC	0.888	0.898	0.866	0.952	1.014	0.101	0.623	0.770	0.516	0.831
Erzikan	LQ	0.709	0.728	0.504	0.670	0.722	0.246	0.411	0.437	0.749	0.563
	NC	0.728	0.754	0.485	0.670	0.783	0.240	0.404	0.435	0.761	0.596
	PC	0.754	0.786	0.460	0.698	0.809	0.231	0.388	0.435	0.776	0.612

are not very different for the LQ and NC cases. This is partly because these failure probabilities are evaluated over the *entire model space*, and the favorable performance achieved with one set of model parameters may not extend to others.

Meanwhile, the PC cases do improve significantly on the total failure probability, by about 5% and 6% for the four- and eight-actuator cases, respectively. It is interesting that this is the case, even though the failure rates for the PC cases, evaluated on the nominal model, are much worse than those of the LQ and NC cases.

It is also worth noting the striking result that the total failure probabilities for the 4PC and 8LQ cases are the same. This emphasizes the interdependency between control law synthesis and actuator design.

### 5.2. Performance in transient response

Tables II–V show the evaluation of performance variables  $J_1$ – $J_{10}$  for the seven earthquake records under consideration. For each of these records, separate results are shown for the cases with the fault parallel to the  $x$ -axis (i.e. FP- $x$ ) and parallel to the  $y$ -axis.

To distill this extensive amount of data down to a few general observations, it is instructive to examine the failure data for each earthquake; i.e. the maximum ratios of  $y_i/\beta_i$  for each failure

Table III. Performance data for FP- $y$  case (four actuators).

Simulation case		$J_1$	$J_2$	$J_3$	$J_4$	$J_5$	$J_6$	$J_7$	$J_8$	$J_9$	$J_{10}$
Newhall	LQ	0.721	0.745	0.683	0.774	0.818	0.271	0.595	0.639	0.693	0.709
	NC	0.713	0.737	0.631	0.745	0.795	0.297	0.547	0.599	0.711	0.688
	PC	0.706	0.729	0.592	0.717	0.771	0.309	0.499	0.568	0.726	0.663
Slymar	LQ	0.662	0.649	0.672	0.647	0.687	0.209	0.451	0.447	0.736	0.640
	NC	0.658	0.642	0.643	0.632	0.685	0.211	0.425	0.439	0.756	0.632
	PC	0.663	0.651	0.624	0.634	0.682	0.209	0.412	0.442	0.771	0.636
El Centro	LQ	0.792	0.796	0.651	0.801	0.804	0.304	0.449	0.478	0.655	0.762
	NC	0.783	0.786	0.630	0.792	0.794	0.330	0.428	0.475	0.678	0.768
	PC	0.765	0.767	0.603	0.773	0.774	0.375	0.417	0.471	0.706	0.764
Rinaldi	LQ	0.845	0.891	0.710	0.928	0.937	0.184	0.401	0.377	0.692	0.925
	NC	0.839	0.885	0.701	0.921	0.931	0.202	0.378	0.358	0.711	0.921
	PC	0.833	0.878	0.693	0.914	0.925	0.203	0.354	0.348	0.727	0.914
Kobe	LQ	0.842	0.843	0.578	0.862	0.865	0.229	0.524	0.576	0.565	0.823
	NC	0.839	0.838	0.570	0.852	0.857	0.242	0.496	0.563	0.581	0.823
	PC	0.836	0.834	0.559	0.848	0.851	0.265	0.468	0.553	0.595	0.812
Jiji	LQ	0.776	0.767	0.893	0.732	0.741	0.101	0.671	0.632	0.500	0.777
	NC	0.774	0.760	0.888	0.751	0.790	0.101	0.668	0.644	0.512	0.784
	PC	0.775	0.782	0.885	0.804	0.851	0.101	0.667	0.661	0.522	0.849
Erzikan	LQ	0.660	0.661	0.576	0.678	0.698	0.230	0.472	0.399	0.725	0.602
	NC	0.656	0.658	0.551	0.686	0.709	0.232	0.441	0.382	0.749	0.596
	PC	0.664	0.675	0.540	0.728	0.779	0.229	0.425	0.377	0.767	0.638

Table IV. Performance data for FP- $x$  case (eight actuators).

Simulation case		$J_1$	$J_2$	$J_3$	$J_4$	$J_5$	$J_6$	$J_7$	$J_8$	$J_9$	$J_{10}$
Newhall	LQ	0.774	0.787	0.601	0.747	0.729	0.382	0.349	0.517	0.735	0.754
	NC	0.756	0.767	0.595	0.725	0.707	0.439	0.355	0.507	0.751	0.735
	PC	0.719	0.728	0.593	0.682	0.666	0.536	0.376	0.490	0.760	0.701
Slymar	LQ	0.735	0.742	0.640	0.708	0.810	0.357	0.382	0.517	0.768	0.730
	NC	0.696	0.698	0.591	0.640	0.763	0.415	0.354	0.475	0.791	0.659
	PC	0.619	0.613	0.593	0.561	0.693	0.490	0.327	0.412	0.805	0.573
El Centro	LQ	0.776	0.754	0.449	0.661	0.685	0.354	0.391	0.396	0.699	0.493
	NC	0.703	0.679	0.416	0.589	0.616	0.474	0.347	0.357	0.730	0.448
	PC	0.608	0.582	0.395	0.506	0.535	0.648	0.329	0.321	0.746	0.383
Rinaldi	LQ	0.885	0.888	0.618	0.882	0.906	0.289	0.373	0.464	0.746	0.802
	NC	0.867	0.870	0.600	0.866	0.891	0.323	0.340	0.422	0.766	0.792
	PC	0.826	0.830	0.586	0.829	0.856	0.402	0.299	0.390	0.776	0.766
Kobe	LQ	0.642	0.636	0.419	0.631	0.858	0.319	0.383	0.397	0.643	0.653
	NC	0.630	0.624	0.410	0.610	0.860	0.373	0.329	0.386	0.660	0.632
	PC	0.560	0.554	0.409	0.596	0.843	0.494	0.296	0.380	0.679	0.599
Jiji	LQ	0.828	0.836	0.905	0.881	0.937	0.216	0.589	0.664	0.622	0.772
	NC	0.827	0.836	0.934	0.892	0.951	0.216	0.629	0.658	0.609	0.778
	PC	0.804	0.816	0.980	0.882	0.945	0.222	0.666	0.658	0.587	0.771
Erzikan	LQ	0.716	0.739	0.461	0.713	0.728	0.381	0.363	0.405	0.798	0.567
	NC	0.681	0.704	0.435	0.703	0.720	0.440	0.334	0.376	0.811	0.548
	PC	0.601	0.615	0.384	0.630	0.656	0.528	0.292	0.325	0.823	0.485

criterion. Because the performance variables  $J_i$  in the tables are all normalized by the uncontrolled values for the structure, these ratios are difficult to determine from the data. Rather than present a battery of additional tables, trends for these ratios can be easily seen from Figure 3, which shows scatter plots for the data. Plots (a) and (b) are for the four-actuator case, while plots (c) and (d) are for the eight-actuator case. Plot (a) shows the maximum normalized quantities for inter-storey drifts vs base drifts, while plot (b) shows the maximum normalized quantities for accelerations vs forces  $\mathbf{f}_c$  (i.e. the maximum over all actuator forces divided by  $f_{\max}$ ). Note that the accelerations and inter-storey drifts stay well below their failure thresholds for all simulations. (Although not explicitly treated as a form of failure, the shear levels of the simulations are also well within safe limits.) It is therefore clear that this benchmark problem essentially distills down to a trade-off between base drift and actuator force.

Now, we return to the data in the tables. Note that  $J_3$  represents the maximum base drift, normalized by the uncontrolled value, and  $J_6$  represents the maximum actuator force, normalized by the total base shear for the controlled structure. From the scatter plots in Figure 3, these two performance measures represent the essential trade-off between different controllers. However, because  $J_6$  is normalized by the total base shear of the *controlled structure*, it cannot be used to directly compare maximum force levels.

Table V. Performance data for FP-y case (eight actuators).

Simulation case		$J_1$	$J_2$	$J_3$	$J_4$	$J_5$	$J_6$	$J_7$	$J_8$	$J_9$	$J_{10}$
Newhall	LQ	0.711	0.735	0.590	0.732	0.785	0.314	0.463	0.561	0.731	0.678
	NC	0.685	0.708	0.575	0.665	0.733	0.409	0.458	0.536	0.748	0.629
	PC	0.639	0.660	0.561	0.589	0.674	0.555	0.457	0.514	0.764	0.559
Slymar	LQ	0.671	0.653	0.626	0.638	0.686	0.292	0.408	0.442	0.779	0.636
	NC	0.626	0.605	0.569	0.600	0.679	0.366	0.349	0.387	0.806	0.625
	PC	0.543	0.528	0.570	0.582	0.662	0.475	0.308	0.318	0.819	0.606
El Centro	LQ	0.735	0.736	0.569	0.743	0.742	0.428	0.371	0.463	0.730	0.767
	NC	0.711	0.712	0.552	0.722	0.720	0.469	0.366	0.447	0.748	0.739
	PC	0.642	0.643	0.528	0.654	0.650	0.583	0.376	0.412	0.765	0.674
Rinaldi	LQ	0.837	0.882	0.695	0.918	0.929	0.260	0.349	0.353	0.746	0.919
	NC	0.809	0.853	0.680	0.890	0.905	0.308	0.320	0.319	0.762	0.896
	PC	0.761	0.802	0.665	0.844	0.864	0.412	0.301	0.287	0.771	0.848
Kobe	LQ	0.827	0.824	0.541	0.836	0.840	0.306	0.422	0.544	0.611	0.807
	NC	0.753	0.746	0.523	0.754	0.768	0.343	0.388	0.533	0.639	0.752
	PC	0.649	0.638	0.509	0.652	0.680	0.505	0.363	0.527	0.670	0.659
Jiji	LQ	0.719	0.717	0.867	0.710	0.717	0.218	0.579	0.550	0.632	0.741
	NC	0.726	0.731	0.913	0.747	0.776	0.216	0.597	0.557	0.638	0.797
	PC	0.720	0.719	0.968	0.765	0.814	0.217	0.629	0.562	0.625	0.822
Erzikan	LQ	0.668	0.671	0.536	0.700	0.721	0.320	0.406	0.371	0.780	0.609
	NC	0.604	0.615	0.476	0.641	0.659	0.412	0.341	0.314	0.804	0.571
	PC	0.523	0.524	0.427	0.555	0.580	0.524	0.307	0.257	0.809	0.504

Consider first the cases corresponding to four actuators. For every earthquake in Tables II and III, the NC and PC controllers incrementally improve upon  $J_3$  in comparison with the LQ case. Meanwhile, the trend in  $J_6$  is less clear. Also note that the high values associated with the Jiji record are due to heavy force saturation for these cases. Consequently, there does not appear to be a lot of difference between the different controllers for this earthquake, in the sense that they all perform poorly due to a deficiency in the necessary force level.

Consider now the case with eight actuators; i.e. Tables IV and V. For these cases, results for  $J_3$  are similar, except that all values are lower. This is due to the fact that the total force capability is now twice what it was for the four-actuator case. The trend in incremental improvement for the LQ, NC, and PC controllers remains. The exception to this is the Jiji earthquake, where again force saturation produces abnormal results, with the LQ controller actually out-performing the others. It is interesting that in comparison to the four-actuator case, the  $J_3$  values for Jiji are actually higher, even though the force capability has been doubled. Compared with using four actuators, there is also a more consistent behavior for  $J_6$  for the eight-actuator case, with incremental increases between the LQ, NC, and PC cases.

It is not clear that there is a significant incremental benefit between using four and eight actuators. Of course, the base drift is noticeably lower for the eight-actuator case, but

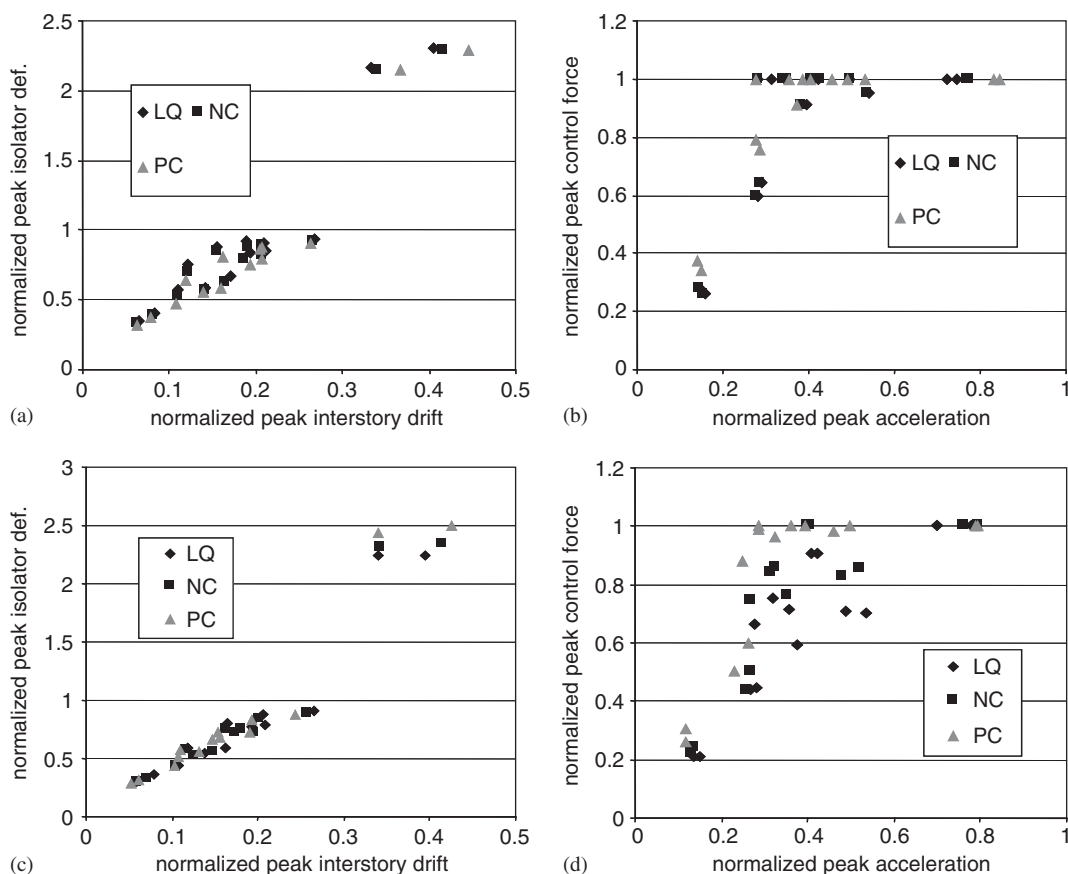


Figure 3. Scatter plots of normalized failure quantities for four actuators (a,b) and eight actuators (c,d) for the 14 ground motion cases.

it is a matter of debate as to whether this marginal improvement justifies the expense of doubling the actuator force capability. It is also an interesting to compare  $J_3$  in the 4PC and 8LQ cases, as was done in the previous subsection. In half the simulations, the PC case with four actuators either performs comparable with, or out-performs, the LQ controller with eight actuators. This further illustrates the interrelation between control optimization and actuator design.

A comparison between  $J_{10}$  (maximum normalized inter-storey corner drift) and  $J_4$  (maximum drift of the center of mass) gives some indication of the degree to which twisting has been suppressed in the structure by the control. Although results are mixed, an underlying observation can be made. For the four-actuator case,  $J_4$  and  $J_{10}$  are usually very close for the PC case (discounting the heavily saturated Jiji responses), implying that the controller suppresses the twisting and the lateral drift by roughly the same amount. However, for the eight-actuator case, the response data is less consistent; sometimes  $J_{10}$  is well below  $J_4$ , while other times it is much greater.

In this paper, the performance for the PC case is compared against a fixed-structure LQ controller using the same optimization weights, and it is believed that this comparison presents the clearest interpretation of the relationship between probabilistic controllers and linear quadratic ones. However, the results presented here can also be compared with those obtained with the LQG active controller presented in the part II of the problem definition [18], which uses the same eight-actuator configuration used in this paper. Discounting the Jiji record, the values of  $J_1$ – $J_5$ ,  $J_7$ , and  $J_8$  are at least 10% lower for the results presented here, even for the four-actuator case, and are significantly lower for the eight-actuator case. The remaining metrics (i.e.  $J_6$  and  $J_9$ ), which are related to force magnitude, are significantly higher, but still below unity for all records. Thus, the controller in [18] simply strikes a different balance between forces and structural reliability.

## 6. CONCLUSIONS

In this paper, a reliability-based active control synthesis method has been described, and has been applied to the benchmark base isolation structural control problem. The intent of this paper has been to demonstrate the concept of reliability-based control in the context of a practical civil engineering problem, and to illustrate the potential value of this control approach. Simulation results imply that this method does indeed yield superior reliability, relative to a comparable LQ controller.

There are clearly many theoretical questions concerning these methods which are not addressed by this paper, and here we suggest only four of the most obvious as items requiring further study. First, as discussed in Section 2, failure criteria must be assigned in such a manner that the correlation between them is low, and this requires more formality than has been presented here. Second, the nonconvexity of failure probability with respect to control parameters presents challenges for the global optimization of these controllers. Third, the optimal-reliability controllers studied in this paper were optimized over a fixed controller domain  $\mathcal{H}$ , and an interesting question concerns the dependency of the optimal reliability on the controller class chosen. Finally, there are clearly unanswered questions regarding the robustness of optimal-reliability active controllers based on linear dynamics, in the presence of nonlinearities such as saturation. Significant further research is necessary to address these issues.

## REFERENCES

1. Housner GW, Bergman LA, Caughey TK, Cassiakos AG, Claus RO, Masri SF, Skelton RE, Soong TT, Spencer BF, Yao JTP. Structural control: past, present and future. *Journal of Engineering Mechanics* 1997; **123**(9):897–971.
2. Spencer BF, Nagarajaiah S. State of the art in structural control. *Journal of Structural Engineering (ASCE)* 2003; **129**(7):845–856.
3. Yamada K, Kobori T. Fundamental dynamics and control strategies for aseismic structural control. *International Journal of Solids and Structures* 2001; **38**(34–35):6079–6121.
4. Narashiman S, Nagarajaiah S, Johnson EA, Gavin HP. Smart base isolated benchmark building part I: problem definition. *Journal of Structural Control and Health Monitoring* 2006.
5. Marrison C, Stengel R. Stochastic robustness synthesis applied to a benchmark problem. *International Journal of Robust and Nonlinear Control* 1995; **5**(1):13–31.
6. Stengel R, Ray L. Stochastic robustness of linear time-invariant control systems. *IEEE Transactions on Automatic Control* 1991; **36**:82–87.
7. Stengel R, Ray L, Marrison C. Probabilistic evaluation of control-system robustness. *International Journal of Systems Science* 1995; **26**(7):1363–1382.

8. Spencer BF, Sain MK, Won C-H, Kaspari DC, Sain PM. Reliability-based measures of control robustness. *Structural Safety* 1994; **15**:111–129.
9. May BS, Beck JL. Probabilistic control for the active mass driver benchmark structural model. *Earthquake Engineering and Structural Dynamics* 1998; **27**(11):1331–1346.
10. Yuen KV, Beck JL. Reliability-based robust control for uncertain dynamical systems using feedback of incomplete noisy response measurements. *Earthquake Engineering and Structural Dynamics* 2003; **32**(5):751–770.
11. Lin YK. *Probabilistic Theory of Structural Dynamics*. Robert E. Krieger Publishing Company: Malabar, FL, 1976.
12. Lutes LD, Sarkani S. *Stochastic Analysis of Structural and Mechanical Vibrations*. Prentice-Hall: Upper Saddle River, NJ, 1997.
13. Veneziano D, Grigoriu M, Cornell CA. Vector-process models for system reliability. *Journal of Engineering Mechanics* 1977; **103**(3):441–460.
14. Papadimitriou C, Beck JL, Katafygiotis LS. Asymptotic expansions for reliabilities and moments of uncertain dynamic systems. *Journal of Engineering Mechanics* 1997; **123**:1219–1229.
15. *Matlab User's Guide*. The Math Works, Inc.: Natick, MA, 1994.
16. *Simulink User's Guide*. The Math Works, Inc.: Natick, MA, 1994.
17. Syrmos VL, Abdallah CT, Dorato P, Grigoriadis K. Static output feedback—a survey. *Automatica* 1997; **33**(2): 125–137.
18. Nagarajaiah S, Narashiman S. Phase I smart base isolated benchmark building—sample controllers for linear isolation system; part II. *Journal of Structural Control and Health Monitoring* 2006.